Halilsarpite, a new arsenate analogue of walentaite, from the Oumlil mine, Bou Azzer district, Morocco

Article *in* European Journal of Mineralogy · January 2020

DOI: 10.5194/ejm-32-89-2020

CITATIONS
6

READS
366

9 authors, including:

Tomas Husdal

21 PUBLICATIONS **108** CITATIONS

SEE PROFILE

Henrik Friis

University of Oslo

76 PUBLICATIONS **425** CITATIONS

SEE PROFILE

Fabrice Dal Bo

University of Liège

54 PUBLICATIONS **145** CITATIONS

SEE PROFILE

Eur. J. Mineral., 32, 89–98, 2020
https://doi.org/10.5194/ejm-32-89-2020

European Journal of Mineralogy
Open Access

Halilsarpite, a new arsenate analogue of walentaite, from the Oumlil mine, Bou Azzer district, Morocco

Tomas Husdal[1], Ian E. Grey[2], Henrik Friis[1], Fabrice Dal Bo[1], Anthony R. Kampf[3], Colin M. MacRae[2], W. Gus Mumme[2], Ole-Thorstein Ljøstad[4], and Finlay Shanks[5]

[1]Natural History Museum, University of Oslo, P.O. Box 1172, Blindern, 0318 Oslo, Norway
[2]CSIRO Mineral Resources, Private Bag 10, Clayton South, Victoria 3169, Australia
[3]Mineral Sciences Department, Natural History Museum of Los Angeles County, 900 Exposition Boulevard, Los Angeles, CA 90007, USA
[4]Elgveien 30, 2406 Elverum, Norway
[5]School of Chemistry, Monash University, Clayton, Victoria 3800, Australia

Correspondence: Ian E. Grey (ian.grey@csiro.au)

Received: 16 August 2019 – Revised: 28 November 2019 – Accepted: 4 December 2019 – Published: 23 January 2020

Abstract. Halilsarpite, $[Mg(H_2O)_6][CaAs_2^{3+}(Fe_{2.67}^{3+}Mo_{0.33}^{6+})(AsO_4)_2O_7]$, is a new secondary mixed arsenate/arsenite mineral from the Oumlil mine, Bou Azzer district, Morocco. It forms lemon-yellow spherules, about 0.1 mm in diameter, composed of platelets, some tens of micrometres in diameter but only 1–2 µm thick. The platelets are flattened on {100} and exhibit perfect cleavage on {100}. The calculated density is 2.89 g cm^{-3}. Optically, halilsarpite is biaxial (−), with $\alpha = 1.646$(calc), $\beta = 1.765(5)$, $\gamma = 1.815(5)$ (white light), and 2V (meas.) = 62(1)°. The partial orientation is $X = \boldsymbol{a}$. Dispersion is weak with $r < v$, and pleochroism is in shades of yellow, $X < Y \approx Z$. Electron microprobe analyses coupled with crystal-structure refinement results give the empirical formula $[(Mg_{0.42}Ca_{0.19}Fe_{0.11}^{3+}\ \square_{0.28})_{\Sigma 1.00}\ (H_2O)_6][((Ca_{0.5}Mg_{0.2}Na_{0.11}\square_{0.14})_{\Sigma 0.95}\ (As^{3+})_{2.05})_{\sum 3.00}(Fe_{2.44}^{3+}\ Mo_{0.56}^{6+})_{\Sigma 3.00}\ ((As_{0.985}^{5+}P_{0.015}^{5+})_{\Sigma 1.00}O_4)_2O_{6.9}(OH)_{0.1}]$. Halilsarpite is orthorhombic, *Imma*, with $a = 26.4890(10)$, $b = 7.4205(3)$, $c = 10.4378(4)$ Å, $V = 2051.67(14)$ Å^3, and $Z = 4$. The structure was solved and refined using single-crystal X-ray data to $wR_{obs} = 0.046$ for 1402 unique reflections to a resolution of 0.75 Å. Halilsarpite is isostructural with walentaite and natrowalentaite, which have structures based on heteropolyhedral layers of configuration $[M1(M2)_2(TO_4)_2(O,OH)_6]$ with surface-attached $As^{3+}O_3$ groups and Ca and Na cations, and with interlayer hydrated cations and H_2O molecules. The octahedrally coordinated sites $M1$ and $M2$ are occupied by Fe^{3+} in walentaite, while $M2 = Fe_{0.67}^{3+}W_{0.33}^{6+}$ in natrowalentaite. Walentaite and natrowalentaite are phosphates, with $T = P^{5+}$. Halilsarpite differs from these minerals in having $T = As^{5+}$ and in having partial replacement of Fe^{3+} by Mo^{6+} in the $M2$-centred octahedra.

1 Introduction

Walentaite, $[Mn^{2+}(H_2O)_6][\square As_3^{3+}Fe_3^{3+}(PO_4)_2O_7]$, from the White Elephant Mine, Pringle, South Dakota (Dunn et al., 1984), and a tungsten-bearing walentaite from the Griffins Find gold deposit, Western Australia (Nickel, 1987), were both originally described as secondary calcium–iron–arsenate–phosphate minerals, with very similar powder X-ray diffraction (PXRD) patterns and optical properties. Recent single-crystal structure analyses and new electron microprobe (EMP) analyses, however, have shown that the As is trivalent in these minerals (Grey et al., 2019a, b) and that the tungsten-bearing walentaite has Na > Ca, leading to its approval by the Commission on New Minerals, Nomenclature and Classification (CNMNC) of the International Mineralogical Association (IMA) as the new mineral natrowalentaite, $[Fe_{0.5}Na_{0.5}(H_2O)_6][NaAs_2^{3+}Fe_{2.33}^{3+}W_{0.67}^{6+}(PO_4)_2O_7]$ (Grey et al., 2018, 2019b). The two minerals are isostructural, with orthorhombic symmetry, space group *Imma*, and with $a \approx 26$ Å, $b \approx 7.3$ Å, and

$c \approx 10.4$ Å. The structures are based on heteropolyhedral layers of configuration $[M1(M2)_2(TO_4)_2(O,OH)_6]$ parallel to (100) with interlayer hydrated cations $A(H_2O)_6$ and H_2O molecules holding the layers together by hydrogen bonding. The layers have B cations and $As^{3+}O_3$ trigonal pyramids coordinated to the surfaces of the layers. Within the layers, the two independent octahedrally coordinated sites, $M1$ and $M2$, are both occupied by Fe^{3+} in walentaite, whereas in natrowalentaite, one-third of the Fe in the $M2$ site is replaced by W^{6+}. The dominant surface-coordinated B cation is Ca in walentaite but Na in natrowalentaite. The interlayer hydrated cation polyhedra are of two types, isolated octahedra centred at site $A1$ and edge-sharing square antiprisms centred at site $A1'$. The octahedra are occupied mainly by Mn^{2+} and Fe^{2+} in walentaite and by Fe^{3+} in natrowalentaite, whereas the antiprisms are occupied mainly by Ca in walentaite and Na in natrowalentaite. The $A1$ and $A1'$ sites are separated by only ~ 1.2 Å so their occupations are mutually exclusive. The tetrahedrally coordinated T site is occupied predominantly by P^{5+} in both minerals. Their general structural formula is $[A1_yA1'_{1-y}(H_2O)_6][B_x(As2)_{2-x}(As3)O][M1(M2)_2(TO_4)_2(O,OH)_6]$, where the three bracketed components correspond to the interlayer hydrated cation sites, the surface-attached sites, and the heteropolyhedral layer sites. Grouping the surface-attached oxygen with the layer anions simplifies the formula to $[A1_yA1'_{1-y}(H_2O)_6][B_x(As2)_{2-x}(As3)M1(M2)_2(TO_4)_2(O,OH)_7]$.

In a study of secondary iron arsenate minerals from the Oumlil mine, Bou Azzer district, Morocco, we identified a new magnesium–calcium–iron–molybdenum–arsenite/arsenate mineral with a PXRD pattern matching that of walentaite. A single-crystal diffraction study on the mineral confirmed that it is isostructural with walentaite, but it has As^{5+} replacing P^{5+} at the T site, as well as minor replacement of Fe^{3+} by Mo^{6+} at the $M2$ site, and with Mg dominant at the A sites.

The new mineral and its name, halilsarpite, were approved by the IMA-CNMNC (IMA2019-023). The name honours mineralogist Halil Sarp born (1944) at Karacasu in Turkey. He completed his education at the University of Geneva in Switzerland and became the curator at the Department of Mineralogy at the Natural History Museum in Geneva. Dr. Sarp also held the Chair of Mineralogy at the University of Geneva. He has published over 100 papers on mineralogy and described over 40 new mineral species, with particular emphasis on secondary copper arsenate minerals. He has made major contributions to the mineralogy of secondary minerals at the Cap Garonne Pb–Cu deposit in France with the characterization of 11 new species including the copper arsenate minerals geminite, mahnerite, pradetite, pushcharovskite, and zdenekite.

The holotype sample has been deposited at the Natural History Museum, University of Oslo, Norway, with the registration number Knr. 44110. Crystals from the holotype are deposited as the cotype in the collections of the Natural History Museum of Los Angeles County, 900 Exposition Boulevard, Los Angeles, CA 90007, USA, catalogue number 73567.

2 Occurrence and associated minerals

Halilsarpite was identified in a small number of hand specimens collected in the Oumlil mine, Bou Azzer district, southern Morocco (30°31′22″ N, 6°47′6″ W), in 2012. The Bou Azzer mining district is one of the world's main Co producers from Co–Ni–Fe arsenide ores. The arsenide ore minerals include löllingite ($FeAs_2$), safflorite ($(Co,Ni,Fe)As_2$), skutterudite ($CoAs_3$), and arsenopyrite (FeAsS), associated with Neoproterozoic peridotite and quartz diorite intrusions in more than 60 orebodies of which the Oumlil deposit is one (Ahmed et al., 2009). Intense weathering of the arsenides has resulted in the formation of a diverse series of secondary ferric arsenite and arsenate minerals including arseniosiderite, karibibite, pharmacosiderite, scorodite, and walentaite (Favreau and Dietrich, 2006).

Halilsarpite spherules occur on resinous brown smolyaninovite (Fig. 1) and brown karibibite. Electron microprobe analysis of the smolyaninovite gave the formula $Ca_{1.1}Co_{0.9}Fe^{3+}_{2.7}(AsO_4)_4 \cdot 11H_2O$. Other associated minerals are Al-rich scorodite, karibibite, and pharmacosiderite, all of which are older than halilsarpite. Safflorite and skutterudite occur as inclusions in the hand specimens. The safflorite is heavily altered and may be the source for As and Fe in the formation of halilsarpite. No primary source of Mo was located in the hand specimens, but both molybdenite and powellite, $CaMoO_4$, occur at Bou Azzer (Favreau and Dietrich, 2006). Yellow crystals and spherules of walentaite or walentaite-like minerals with variable chemistry have been found on several occasions at the Oumlil mine and nearby localities (Georges Favreau, personal communication, 2019), but only the present material has been identified as halilsarpite.

3 Physical and optical properties

Halilsarpite forms lemon-yellow spherules, about 0.1 mm in diameter (Fig. 2). Scanning electron microscope (SEM) inspection of the spherules showed that they are composed of layers of platelets, some tens of micrometres in diameter but only 1–2 µm thick (Fig, 3). The plane of the platelets is {100} and this was the only discernible form. The platelets have a vitreous lustre and are brittle with perfect {100} cleavage. The calculated density is 2.89 g cm^{-3}, based on the empirical formula and PXRD cell.

Optically, halilsarpite is biaxial (–), with the indices of refraction $\alpha = 1.646$(calc), $\beta = 1.765(5)$, and $\gamma = 1.815(5)$, measured in white light. The 2V (meas.) $= 62(1)°$ from extinction data using EXCALIBR (Gunter et al., 2004). Dispersion is weak with $r < v$. The optical orientation could only

Figure 1. Yellow spherules of halilsarpite on orange-brown smolyaninovite from the Oumlil mine, Morocco. FOV 3.15 mm. Photo by Ole-Thorsein Ljøstad.

Figure 2. Spherules of halilsarpite, FOV 0.7 mm. Photo by Ole-Thorstein Ljøstad.

be partially determined as $X = \boldsymbol{a}$. The pleochroism involves shades of yellow, with $X < Y \approx Z$. Because X is perpendicular to the very thin plates, α could not be measured; consequently, it has been calculated from β, γ, and 2V. The tiny plates exhibited uniform extinction, although they generally consist of multiple slightly offset plates. The Gladstone–Dale compatibility, 1-(K_P/K_C) (Mandarino, 2007), is −0.042 (GOOD) based upon the empirical formula and density calculated using the powder XRD unit cell and the indices of refraction.

4 Raman spectroscopy

A Raman spectrum on crystal aggregates was obtained using a Renishaw inVia Raman microscope with 514.5 nm argon green laser excitation and a Leica short-working-distance objective. A 90 µm slit was employed. The power at the sample was approximately 0.5 mW and the accumulation time was 30 s.

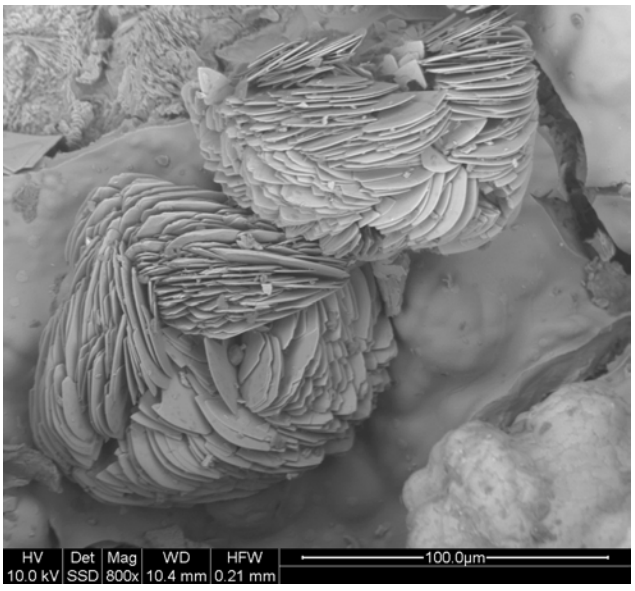

Figure 3. Backscattered electron image of halilsarpite spherules.

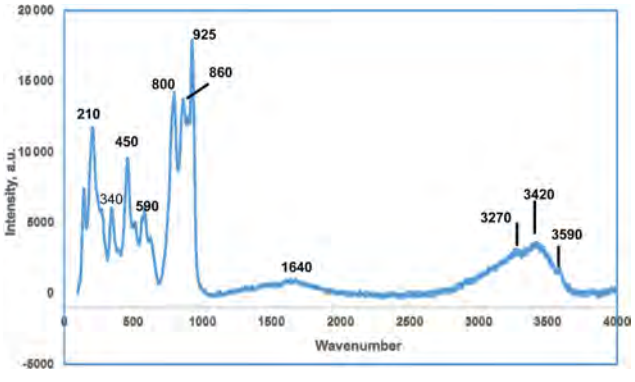

Figure 4. Raman spectrum for halilsarpite.

The Raman spectrum in the range from 20 to 4000 cm^{-1} is shown in Fig. 4. In the O–H stretching region, a broad band with peaks at 3270 and 3420 cm^{-1} corresponds to H-bonded H_2O while a weak sharp peak at 3590 cm^{-1} is most likely due to hydroxyl groups. A broad H–O–H bending mode vibration is centred at 1640 cm^{-1}. The halilsarpite crystal structure comprises layers of FeO_6 octahedra and AsO_4 tetrahedra that have the same topology as jarosite-group minerals, specifically segnitite, $PbFe_3(AsO_4)(AsO_3OH)(OH)_6$. Therefore, the As^{5+}–O and Fe^{3+}–O Raman spectra peaks below 1000 cm^{-1} were interpreted with the aid of publications of Raman spectra by Sasaki et al. (1998) on jarosite minerals and Frost et al. (2005) on segnitite. The interpretation is complicated by the presence of peaks due to Mo^{6+}–O and As^{3+}–O stretching vibrations, which overlap with As^{5+}–O peaks. For Mo^{6+}–O and As^{3+}–O peaks, the publication by Cejka et al. (2010) on the Raman spectrum of vajdakite, $[(Mo^{6+}O_2)_2(H_2O)_2As_2^{3+}O_5] \cdot H_2O$, was helpful. On the ba-

Table 1. Analytical data (wt%) for halilsarpite.

Constituent	Mean	Range	SD	Reference material
Na_2O	0.36	0.23–0.48	0.07	albite
K_2O	0.04	0.0–0.11	0.04	adularia
MgO	2.74	2.18–3.19	0.36	$MgAl_2O_4$
CaO	4.25	3.74–4.77	0.32	wollastonite
Fe_2O_3[a]	22.3	18.6–24.3	1.6	hematite
MoO_3	8.83	7.8–10.1	0.6	$CaMoO_4$
P_2O_5	0.25	0.13–0.41	0.09	$AlPO_4$
As_2O_3	22.2	20.5–24.1	1.2	scorodite
As_2O_5	24.7	22.9–26.9	1.4	scorodite
H_2O[b]	12.2			
Total	97.9			

[a] Total Fe as Fe_2O_3, based on the crystal structure. [b] H_2O calculated based on 6 H_2O pfu, from the crystal structure.

sis of these studies, the peak at 925 cm^{-1} is an Mo^{6+}–O stretching vibration, while that of As^{5+}–O is at 860 cm^{-1} and As^{3+}–O is at 800 cm^{-1}. Other stretching vibrations due to these species are unresolved in the envelope from 700 to 1000 cm^{-1}. The peaks centred around 590 cm^{-1} correspond to both Mo^{6+}–O and As^{3+}–O bending vibrations (Cejka et al., 2010). The band centred at 450 cm^{-1} corresponds to the bending region for AsO_4 (Frost et al., 2005) but also has a contribution from Fe^{3+}–O vibrations. Other Fe^{3+}–O vibrations are at 340 and 210 cm^{-1} (Sasaki et al., 1998).

5 Chemical composition

Halilsarpite crystal aggregates were mounted in a polished section and analysed using wavelength-dispersive spectrometry on a JEOL JXA-8500F Hyperprobe operated at an accelerating voltage of 15 kV and a beam current of 5 nA. The beam was defocused to 5 µm. Standards were scorodite (As), wollastonite (Ca), albite (Na), adularia (K), $AlPO_4$ (P), hematite (Fe), $MgAl_2O_4$ (Mg), and $CaMoO_4$ (Mo). Analytical results (average of 16 analyses) are given in Table 1. The water content is from the crystal structure (to give 6 H_2O pfu). The As_2O_3/As_2O_5 were apportioned to give 2 ($As^{5+} + P$) pfu, consistent with the crystal structure. The slightly low analysis total is most likely due to the thinness of the platelets. For the calculation of the empirical formula, the oxide mass fraction (wt%) values in Table 1 were scaled to give $\Sigma\text{oxides} + H_2O = 100$.

The atomic proportions, normalized to 21 anions, are $Na_{0.11}K_{0.01}Ca_{0.69}Mg_{0.62}Fe^{3+}_{2.55}Mo_{0.56}As^{3+}_{2.05}As^{5+}_{1.97}P_{0.03}O_{21}H_{12.1}$.

Combining the analyses with crystal-structure refinement results gives the empirical formula $[(Mg_{0.42}\ Ca_{0.19}\ Fe^{3+}_{0.11}\ \square_{0.28})_{\Sigma 1.00}\ (H_2O)_6]\ [((Ca_{0.5}\ Mg_{0.2}\ Na_{0.11}\ K_{0.01}\square_{0.13})_{\Sigma 0.95}\ (As^{3+})_{2.05})_{\sum 3.00}\ (Fe^{3+}_{2.44}Mo^{6+}_{0.56})_{\Sigma 3.00}\ ((As^{5+}_{0.985}\ P^{5+}_{0.015})_{\Sigma 1.00}\ O_4)_2\ O_{6.9}(OH)_{0.1}]$.

The simplified formula for halilsarpite is $[(Mg, Ca, Fe^{3+}, \square)\ (H_2O)_6]\ [(Ca, Mg, Na, \square)\ As^{3+}_2(Fe^{3+}, Mo^{6+})_3\ (AsO_4)_2O_7]$.

The ideal formula is $[Mg(H_2O)_6][CaAs^{3+}_2\ (Fe^{3+}_{2.67}Mo^{6+}_{0.33})\ (AsO_4)_2O_7]$, which requires Fe_2O_3 23.89, CaO 6.28, MgO 4.51, MoO_3 5.32, As_2O_3 22.16, As_2O_5 25.74, H_2O 12.10, and total 100.00 wt.%.

6 X-ray crystallography

A 0.1 mm spherule of halilsarpite was used to collect PXRD data with a Rigaku Synergy-S diffractometer equipped with a hybrid photon counting area detector (HyPix6000HE), housed at the Natural History Museum (NHM) in Oslo. Data were collected in the two-theta range 4 to 82° using monochromatized CuKα radiation. A Gandolfi-like motion on the φ and ω axes was used to randomize the sample. Rietveld refinements were made using FullProf (Rodriguez-Carvajal, 1990). Refined orthorhombic unit cell parameters are $a = 26.516(2)$ Å, $b = 7.4036(6)$ Å, $c = 10.4192(12)$ Å, and $V = 2045.5(3)$ Å^3. The indexed PXRD pattern for halilsarpite is given in Table 2.

Single-crystal X-ray studies were carried out with a platelet separated from a rosette of Oumlil mine crystals and mounted on a cryoloop with oil for room temperature data collections using a Rigaku Synergy-S diffractometer with sealed micro-sources (Mo and Cu) and a HyPix-6000HE detector. The data collection, integration, and face absorption corrections were all carried out in Rigaku's CrysAlis Pro software. A 49 h data collection was made at room temperature using MoKα radiation and a detector distance of 34 mm. The data quality was also checked using CuKα radiation at a longer detector distance of 45 mm. This showed that the reflections were multiply split due to contributions from subparallel lamellae. In the Mo dataset, the splitting was minimal, and the reflections were successfully integrated from the whole crystal, giving $R_{\text{int}} = 0.050$ for equivalent reflections. Other details of the data collection are given in Table 3.

Crystal-structure refinement

The atom coordinates for walentaite in space group *Imma* (Grey et al., 2019a) were used to start the refinement, with tetrahedral As^{5+} replacing P^{5+} at the T site. Based on previous experience with refinement of the walentaite and natrowalentaite structures, the metal atoms per formula unit (apfu) from the EMP analyses were distributed at the different metal atom sites in the following way: Mo was ordered, together with Fe at $M2$, Fe was ordered at $M1$, and any remaining Fe was located at the interlayer site $A1$. Ca was distributed between the interlayer $A1'$ site and the surface-attached B site. Mg was distributed uniformly over

Table 2. Powder X-ray data for halilsarpite (d in Å).

I_{obs}	d_{meas}	d_{calc}	h	k	l
100	13.28	13.26	2	0	0
16	9.710	9.696	1	0	1
20	6.737	6.740	3	0	1
18	6.042	6.035	0	1	1
3	5.487	5.493	2	1	1
6	4.849	4.848	2	0	2
33	4.462	4.463	4	1	1
7	3.563	3.566	2	2	0
		3.560	7	0	1
7	3.348	3.370	6	0	2
		3.321	5	1	2
		3.315	8	0	0
1	3.247	3.244	3	2	1
6	3.148	3.144	0	1	3
36	3.018	3.018	0	2	2
11	2.944	2.942	2	2	2
2	2.905	2.905	8	1	1
3	2.834	2.841	4	1	3
		2.831	7	1	2
14	2.799	2.796	8	0	2
5	2.607	2.604	0	0	4
1	2.556	2.556	2	0	4
2	2.473	2.469	8	2	0
3	2.426	2.435	3	2	3
		2.423	9	1	2
2	2.360	2.367	3	1	4
		2.363	10	0	2
7	2.251	2.258	4	3	1
		2.247	9	0	3
2	2.157	2.163	3	3	2
		2.156	10	2	0
2	2.065	2.061	7	1	4
2	2.014	2.012	0	3	3
7	1.984	1.989	2	3	3
		1.980	11	0	3
5	1.922	1.925	4	3	3
		1.919	6	2	4
4	1.851	1.851	0	4	0
7		1.792	8	2	4
3	1.717	1.720	8	3	3
		1.716	8	1	5
3	1.661	1.660	10	2	4
		1.657	16	0	0
2	1.623	1.622	6	4	2
		1.619	6	4	2
2	1.598	1.598	16	1	1
2	1.570	1.572	0	2	6
		1.569	13	1	4
8	1.545	1.546	9	2	5
		1.544	8	4	2

the three sites $A1$, $A1'$, and B. The Ca and Fe (in $A1$) contents were fixed, and the Mg content was refined at the three sites. The Fe and Mo coordinates at the $M2$ site were refined independently and the sum of their occupancies was restrained to full occupancy of the site. The occupancies of split, partially occupied Ow sites in the interlayer region and the split, partially occupied As2 and As3 sites were refined. With anisotropic displacement parameters for the heteropolyhedral-layer atoms and isotropic displacement parameters for the partially occupied interlayer and surface-attached atoms, a refinement using JANA2006 (Petříček et al., 2014) converged to $wR_{obs} = 0.046$ for 1402 unique reflections. Other details of the refinement are given in Table 3. The refined coordinates and equivalent isotropic displacement parameters are reported in Table 4, anisotropic displacement parameters in Table 5, and polyhedron bond distances are given in Table 6. Note that although the 0.50(2) Mg apfu obtained from the site occupancy refinements (Table 4) agrees reasonably with the EMP-derived 0.62 Mg apfu, the site occupancies given in Table 4 for the $A1$, $A1'$, and B sites should be considered with caution because all three sites are occupied by multiple cations as well as vacancies.

7 Discussion

The single-crystal refinement confirms that halilsarpite is isostructural with walentaite (Grey et al., 2019a) and natrowalentaite (Grey et al., 2019b). The main features of the walentaite-type structure are shown in Figs. 5 to 7. A projection of the structure along [010] in Fig. 5 shows undulating heteropolyhedral layers of configuration $[M1(M2)_2(T\mathrm{O}_4)_2(\mathrm{O,OH})_6]$ together with surface-attached B site cations and interlayer hydrated cation octahedra centred at site $A1$. The corresponding interlayer polyhedra centred at site $A1'$ are shown in Fig. 6. These polyhedra have square antiprismatic coordination and share edges to give the composition $A1'(\mathrm{H_2O})_4(\mathrm{H_2O})_{4/2} \equiv A1'(\mathrm{H_2O})_6$. Surface-coordinated $\mathrm{As^{3+}O_3}$ groups centred at sites As2 and As3 are shown in Fig. 7.

Single-crystal refinements for walentaite (Grey et al., 2019a), natrowalentaite (Grey et al., 2019b), and halilsarpite show features that are consistent across the three minerals. The atoms forming the heteropolyhedral layers of configuration $[M1(M2)_2(T\mathrm{O}_4)_2(\mathrm{O,OH})_6]$ are fully ordered in sites of space group *Imma*, whereas the atoms that are attached to the surface of the layers (at sites B, As2, As3, O6) and those occupying sites in the interlayer region ($A1$, $A1'$, Ow atoms) occupy multiply split, partially occupied sites that are generally displaced from special positions in *Imma* and, therefore, for these atoms, the *Imma* structure corresponds to an average structure. For the case of walentaite (Grey et al., 2019a), the structure was refined in various subgroups of *Imma*, coupled with twinning, in an attempt to establish the ordering at the split sites, but without success (ghost images of the

Table 3. Data collection and refinement conditions for halilsarpite.

Atomic proportions (scaled to 21 anions)	$K_{0.01}Ca_{0.69}Mg_{0.62}Fe^{3+}_{2.55}Mo_{0.56}$ $As^{3+}_{2.05}As^{5+}_{1.97}P_{0.03}O_{21}H_{12.1}$
Formula mass	892.1
Temperature	293 K
Wavelength	0.7107 Å
Crystal system, space group	Orthorhombic, *Imma*
Unit cell dimensions	$a = 26.4890(10)$ Å
	$b = 7.4205(3)$ Å
	$c = 10.4378(4)$ Å
Volume	2051.67(14) Å^3
Z, calculated density	4, 2.89 g cm^{-3}
Absorption coefficient	8.84 mm^{-1}
Crystal size	$0.017 \times 0.030 \times 0.051$ mm
Data resolution for refinement	0.75 Å
Reflections collected/unique/observed	8963/1402 [$R_{int} = 0.050$]/1111
Completeness to theta = 29.09°	98 %
Refinement method	Full-matrix least-squares on F
Data/constraints/parameters	1402/0/111
Goodness of fit	2.02
Final R indices [$I > 3$sigma(I)]	$R_{obs} = 0.041$, $wR_{obs} = 0.045$
R indices (all data)	$R_{obs} = 0.055$, $wR_{obs} = 0.046$
Largest diff. peak and hole	1.13 and −0.83 e.Å^{-3}

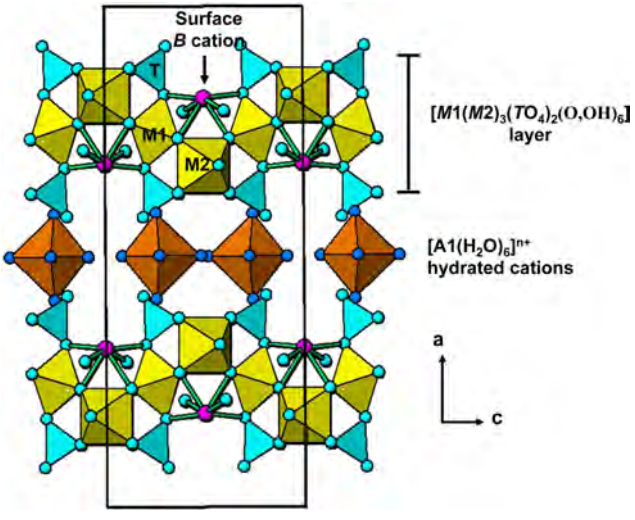

Figure 5. [010] projection of the walentaite structure type.

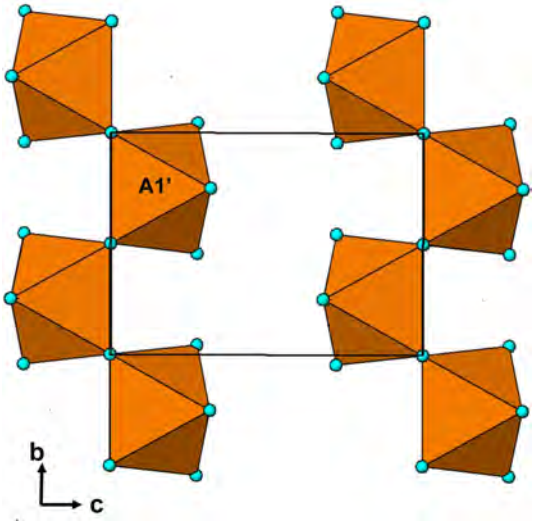

Figure 6. Chains of edge-shared square antiprisms, $A1'(H_2O)_4(H_2O)_{4/2}$, in the interlayer region of walentaite-group minerals.

split atoms occurred). The most likely explanation is that, in the crystals of these minerals, different distributions of the surface-coordinated and interlayer hydrated cations have very similar free energies, and specific distributions are ordered only locally over very small regions.

An unusual feature common to the three minerals is the presence of surface-coordinated trimeric arsenite clusters with the composition $[As^{3+}_3O_6]^{3-}$. The clusters, which have not previously been reported in arsenite minerals, are formed by corner-shared pairs of $(As2)O_3$ pyramids sharing an edge with an $(As3)O_3$ pyramid (see Fig. 7). The three arsenite groups share a common anion, O6, with resulting long As2–O6 and As3–O6 bonds (see Table 6). The bonds for both AsO_3 pyramids are longer than reported for arsenite minerals (Hawthorne, 1985), particularly so for the $(As3)O_3$ pyramid. This can be understood within the context that As^{3+} partially

Table 4. Refined coordinates, equivalent isotropic displacement parameters, and site occupation factors (sof) for halilsarpite.

Atom	Site	sof*	x	y	z	U_{eq} (Å^2)
$[M1(M2)_2\ (TO_4)_2O_6]$ layer						
$M1$	4(c)	0.25 Fe^{3+}	0.25	0.25	0.25	0.0159(3)
$M2$	8(f)	0.373(3) Fe^{3+}	0.32427(16)	0.5	0.5	0.0169(6)
$M2'$		0.127(3) Mo^{6+}	0.3092(2)	0.5244(7)	0.4923(6)	0.0169(6)
T	8(i)	0.5 As^{5+}	0.374258(19)	0.25	0.27928(6)	0.01980(19)
O1	8(i)	0.5	0.42555(16)	0.25	0.1878(5)	0.0356(16)
O2	8(i)	0.5	0.32184(15)	0.25	0.1890(4)	0.0317(15)
O3	16(j)	1	0.37434(10)	0.4339(4)	0.3738(3)	0.0270(10)
O4A	16(j)	0.5	0.2684(3)	0.5457(9)	0.6297(7)	0.0179(9)
O4B	16(j)	0.5	0.2618(2)	0.574(1)	0.6072(7)	0.0179(9)
O5	8(i)	0.5	0.31916(14)	0.25	0.5719(4)	0.0227(13)
Surface-coordinated atoms						
As2	16(j)	0.241(2) As^{3+}	0.21448(7)	0.0300(4)	0.5154(4)	0.0171(11)
As3	16(j)	0.234(2) As^{3+}	0.27130(6)	0.3064(2)	0.69453(17)	0.0185(6)
B	8(f)	0.12Ca +0.032(5)Mg	0.1831(3)	0.010(3)	0.510(3)	0.0429(14)
O6	8(i)	0.267(9)	0.2148(3)	0.25	0.6021(9)	0.035(3)
Interlayer species						
$A1$	4(e)	0.04Fe +0.051(3)Mg	0.0	0.25	0.8017(7)	0.0429(14)
$A1'$	4(e)	0.05Ca +0.043(3)Mg	0.0	0.25	0.6909(9)	0.0429(14)
OW1A	8(i)	0.29(1)	0.5684(4)	0.75	0.3382(16)	0.061(2)
OW1B	8(i)	0.23(1)	0.5814(6)	0.75	0.2696(19)	0.061(2)
OW2A	8(h)	0.32(1)	0.5	0.4645(14)	0.2792(12)	0.061(2)
OW2B	8(h)	0.18(1)	0.5	0.524(3)	0.197(2)	0.061(2)
OW3	8(i)	0.05(1)	0.529(2)	0.75	0.482(6)	0.061(2)
OW4	4(c)	0.05(1)	0.5	0.75	0.094(5)	0.061(2)
OW5	16(j)	0.20(1)	0.4477(8)	0.550(3)	0.034(2)	0.061(2)
OW6	8(i)	0.10(1)	0.3975(11)	0.25	-0.042(3)	0.061(2)

* The sof multiplied by 4 gives the number of atoms per formula unit.

Table 5. Anisotropic displacement parameters (Å^2) for halilsarpite.

Atom	U^{11}	U^{22}	U^{33}	U^{23}	U^{13}	U^{12}
$M1$	0.0196(5)	0.0131(6)	0.0150(7)	0	−0.0001(4)	0
$M2$	0.0258(16)	0.0100(7)	0.0149(6)	0	0	−0.0008(5)
T	0.0194(3)	0.0217(3)	0.0183(3)	0	0.0027(2)	0
As2	0.0209(11)	0.015(2)	0.016(2)	0.0001(6)	−0.0004(7)	−0.0004(11)
As3	0.0275(11)	0.0131(10)	0.0148(11)	0.0024(5)	0.0034(6)	0.0022(6)
O1	0.022(2)	0.050(3)	0.035(3)	0	0.0115(16)	0
O2	0.022(2)	0.051(3)	0.021(3)	0	−0.0006(16)	0
O3	0.0291(15)	0.0175(15)	0.034(2)	−0.0052(12)	0.0066(12)	−0.0022(13)
O5	0.030(2)	0.013(2)	0.024(3)	0	−0.0015(16)	0

occupies multiply split positions at both As2 and As3 sites, and their coordinating anions can be expected to occupy different positions for each combination of As^{3+} positions, although only the weighted centroid of the displaced anions is obtained in the refinement.

In the interlayer region, the two different cation sites, $A1$ and $A1'$, are both special 4(e) sites, (0, 1/4, z) (Table 4), and their separation is only ~ 1.2 Å, so that occupation of the two sites is mutually exclusive. There is evidence from the analysis of site occupancies in walentaite (Grey et al., 2019a) that the occupation of the interlayer sites is correlated

Table 6. Polyhedral distances in halilsarpite (Å).

*M*1	−O2 x2	2.007(4)			
	−O4A x4*	2.027(7)			
	−O4B x4*	2.008(7)			
*M*2	−O3 x2	1.933(4)	*M*2′	−O3 x2	2.228(7), 2.243(6)
	−O4A x2*	2.035(8)		−O4A x2*	1.803(9), 1.750(9)
	−O4B x2*	2.070(8)		−O4B x2*	1.774(9), 1.784(9)
	−O5 x2	2.006(2)		−O5 x2	2.215(6), 1.822(6)
T	−O1	1.661(5)	As2	−O4B	1.756(7)
	−O2	1.678(4)		−O4B	1.820(8)
	−O3 x2	1.684(3)		−O6	1.867(6)
*A*1	−Ow1A x2*	1.85(1)	As3	−O4A	1.901(7)
	−Ow1B x2*	2.18(2)		−O5	1.849(4)
	−Ow2A x2*	2.13(1)		−O6	1.830(9)
	−Ow2B x2*	2.00(2)			
	−Ow3	2.04(7)			
	−Ow4	2.16(6)			
*A*1′	−Ow1A x2*	2.38(1)	*B*	−O2 x2	2.69(2), 2.74(2)
	−Ow1B x2*	2.31(2)		−O4A x2*	2.61(2), 2.70(2)
	−Ow2A x2	2.31(1)		−O4B x2*	2.40(1), 2.46(1)
	−Ow5 x4	2.62(2)		−O6 x2	2.19(2), 2.40(2)
				−Ow6 x2	2.80(3), 2.93(3)

* Disordered atoms *n*A and *n*B cannot both be present in the same polyhedron.

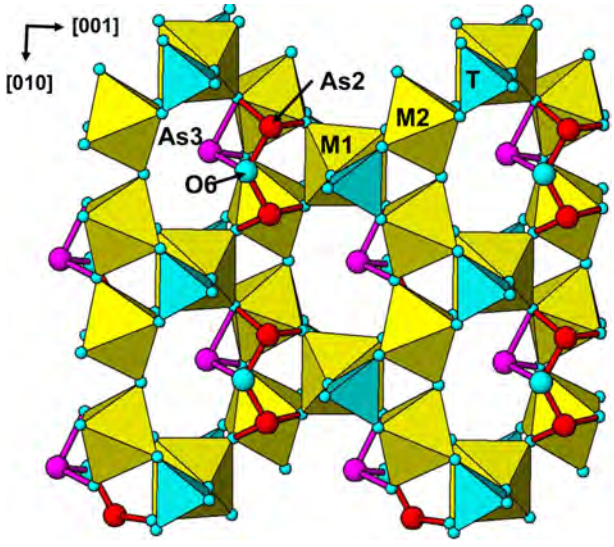

Figure 7. [100] projection of the halilsarpite structure, showing surface-coordinated $As^{3+}O_3$ trigonal pyramids.

with the occupation of the surface-attached species. Specifically, the octahedrally coordinated *A*1 sites are occupied when the As2 sites are occupied and trimeric $(As2)_2(As3)O_6$ clusters are present on the surface, whereas the eight coordinated *A*1′ sites are occupied when the As2 sites are vacant, and $As3O_3$ pyramids and *B* site cations are the surface-coordinated species.

There is also a correlation between the occupancy of the *M*2 site and the occupancies of the As2 and *B* sites, due to the anion valency constraints imposed by the $(As2)O_3$ pyramids sharing edges with the *M*2-centred octahedra, as discussed by Grey et al. (2019b). The As2 and *B* sites are separated by only ∼ 0.9 Å and their occupation is mutually exclusive, as for the *A*1/*A*1′ sites. When the *M*2 site is occupied by Fe^{3+} only, as in walentaite, the As2 site is 80 % occupied and the *B* site (occupied by Ca) is only 20 % occupied. When the Fe^{3+} is partially replaced by Mo^{6+} at the *M*2 site of halilsarpite (or by W^{6+} in natrowalentaite), the As2 site occupancy falls to 50 % and the *B* site occupancy correspondingly increases to 50 % giving $CaAs_2^{3+}$ surface species in halilsarpite and $NaAs_2^{3+}$ species in natrowalentaite. In the refinement of halilsarpite, the Fe^{3+} and Mo^{6+} were found to occupy different positions at the *M*2 site, separated by 0.45 Å. Whereas the Fe^{3+}–O distances are in the narrow range of 1.93 to 2.07 Å (*M*2 in Table 6), the Mo^{6+} has two short bonds 1.75 and 1.80 Å and four longer bonds (*M*2′ in Table 6), typical of octahedrally coordinated Mo^{6+}, for example in MoO_3 (Kihlborg, 1963).

The properties of halilsarpite, walentaite, and natrowalentaite are compared in Table 7. The ideal formulae for the three minerals are

Table 7. Comparison of halilsarpite with walentaite and natrowalentaite.

	Walentaite*	Natrowalentaite	Halilsarpite
Ideal Formula	$[(Mn^{2+}(H_2O)_6][\square As_3^{3+} Fe_3^{3+}(PO_4)_2O_7]$	$[Fe_{0.5}Na_{0.5}(H_2O)_6][NaAs_2^{3+} Fe_{2.33}^{3+}W_{0.67}^{6+}(PO_4)_2O_7]$	$[Mg(H_2O)_6][CaAs_2^{3+} Fe_{2.67}^{3+}Mo_{0.33}^{6+}(AsO_4)_2O_7]$
Symmetry	Orthorhombic, *Imma*	Orthorhombic, *Imma*	Orthorhombic, *Imma*
a (Å)	26.188(5)	25.770(3)	26.4890(10)
b (Å)	7.360(2)	7.3250(8)	7.4205(3)
c (Å)	10.367(2)	10.522(1)	10.4378(4)
V (Å^3)	1998.2(7)	1986.2(4)	2051.67(14)
Strongest powder pattern lines d, I, (hkl)	12.9, 100 (200) 9.6, 15 (101) 6.56, 20 (400) 4.43, 30 (411) 3.00, 50 (022) 2.931, 20 (222) 2.776, 20 (802)	12.95, 100 (200) 9.72, 9 (101) 6.72, 14 (101) 4.41, 10 (411) 3.020, 27 (022) 2.940, 15 (222) 2.759, 11 (802)	13.28, 100, (200) 9.71, 16, (101) 6.737, 20, (301) 4.462, 33, (411) 3.018, 36, (022) 2.944, 11, (222) 2.799, 14, (802)
Optics	Biaxial (+) α = n.d., $\beta = 1.738(4)$, $\gamma = 1.779(4)$, 2V = n.d.	Biaxial (−) $\alpha = 1.650(3)$, $\beta = 1.728(3)$, $\gamma = 1.772(3)$, 2V(meas) = 71(2)°	Biaxial (−) $\alpha = 1.646$ (calc), $\beta = 1.765$ (5), $\gamma = 1.815(5)$, 2V (meas.) = 62(1)°

* Powder lines and optics from Dunn et al. (1984).

$[Mn(H_2O)_6][\square As_3^{3+} Fe_3^{3+} (PO_4)_2 O_7]$ for walentaite,

$[Fe_{0.5} Na_{0.5}(H_2O)_6][NaAs_2^{3+} Fe_{2.33}^{3+} W_{0.67}^{6+} (PO_4)_2 O_7]$ for natrowalentaite, and

$[Mg(H_2O)_6][CaAs_2^{3+} (Fe_{2.67}^{3+} Mo_{0.33}^{6+}) (AsO_4)_2 O_7]$ for halilsarpite.

These are consistent with a general chemical formula for the three minerals given as $[A(H_2O)_6][B_xC_{3-x}]M_3(TO_4)_2(O,OH)_7]$, where A, C, and M include the atoms at $A1 + A1'$, As2 + As3, and $M1 + M2$ sites respectively. Halilsarpite is distinguished principally by having $T = As^{5+}$, whereas walentaite and natrowalentaite have $T = P^{5+}$. The replacement of P^{5+} by the larger As^{5+} in halilsarpite results in a 3 % expansion of the unit cell volume, shown in Table 7. Halilsarpite also differs from the other two minerals in having $A =$ dominant Mg and in having partial replacement of Fe^{3+} by Mo^{6+} in the $M2$ site.

Data availability. Crystallographic data for halilsarpite are available in the Supplement.

Supplement. The supplement related to this article is available online at: https://doi.org/10.5194/ejm-32-89-2020-supplement.

Author contributions. TH conducted preliminary analyses and identified the new mineral as related to walentaite. IEG analysed the experimental data and wrote the paper. HF and FDB carried out the single-crystal and powder XRD experiments. ARK made the optical measurements. CMM performed the EMP analyses. WGM assisted in the crystal structure refinement. OTL provided the specimens and photographed them for Figs. 1 and 2. FS obtained the Raman spectrum.

Competing interests. The authors declare that they have no conflict of interest.

Acknowledgements. Thanks are due to Cameron Davidson and Matt Glenn for EMP sample preparation and scanning electron microscopy help.

Review statement. This paper was edited by Cristian Biagioni and reviewed by Ferdinando Bosi and one anonymous referee.

References

Ahmed, A. H., Arai, S., and Ikenne, M.: Mineralogy and paragenesis of the Co-Ni arsenide ores of Bou Azzer, Anti-Atlas, Morocco. Econ. Geol., 104, 249–266, 2009.

Cejka, J., Bahfenne, S., Frost, R. L., and Sejkora, J.: Raman spectroscopic study of the arsenite mineral vajdakite,

$[(Mo^{6+}O_2)_2(H_2O)_2As_2^{3+}O_5] \cdot H_2O$, J. Raman Spectrosc., 41, 74–77, 2010.

Dunn, P. J., Peacor, D. R., Roberts, W. L., Campbell, T. J., and Ramik, R. A.: Walentaite, a new calcium iron arsenate phosphate from the White Elephant Mine, Pringle, South Dakota, Neues Jahrb. Mineral., Monatsh., 1984, 169–174, 1984.

Favreau, G. and Dietrich, J. E.: Die Mineralien von Bou Azzer, Lapis, 31, 27–68, 2006.

Frost, R. L., Weier, M. L., Martens, W., and Mills, S.: Molecular structure of segnitite: A Raman spectroscopic study, J. Mol. Struct., 752, 178–185, 2005.

Grey, I. E., Mumme, W. G., Kampf, A. R., and MacRae, C. M.: Natrowalentaite, IMA2018-032a. CNMNC Newsletter No. 46, December 2018, p. 1189, Eur. J. Mineral., 30, 1181–1189, 2018.

Grey, I. E., Mumme, W. G., and Hochleitner, R.: Trimeric $As_3^{3+}O_6$ clusters in walentaite: Crystal structure and revised formula, Eur. J. Mineral., 31, 111–116, 2019a.

Grey, I. E., Mumme, W. G., Kampf, A. R., MacRae, C. M., and Wilson, N. C.: Natrowalentaite, a new mineral from the Griffins Find gold deposit, Western Australia, Aust. J. Mineral., 20, 7–15, 2019b.

Gunter, M. E., Bandli, B. R., Bloss, F. D., Evans, S. H., Su, S. C., and Weaver, R.: Results from a McCrone spindle stage short course, a new version of EXCALIBR, and how to build a spindle stage, Microscope, 52, 23–39, 2004.

Hawthorne, F. C.: Schneiderhöhnite, $Fe^{2+}Fe_2^{3+}As_5^{3+}O_{13}$, a densely packed arsenite structure, Can. Mineral., 23, 675–679, 1985.

Kihlborg, L.: Least-squares refinement of crystal structure of molybdenum trioxide, Arkiv. Kemi, 21, 357–364, 1963.

Mandarino, J. A.: The Gladstone–Dale compatibility of minerals and its use in selecting mineral species for further study, Can. Mineral., 45, 1307–1324, 2007.

Nickel, E. H.: Tungsten-bearing walentaite from Griffins Find gold deposit, Western Australia, Aust. Mineral., 1987, 9–12, 1987.

Petříček, V., Dušek, M., and Palatinus, L.: Crystallographic Computing System JANA2006: General features, Z. Kristallogr., 229, 345–352, 2014.

Rodriguez-Carvajal, J.: FULLPROF: A Program for Rietveld Refinement and Pattern Matching Analysis. Satellite meeting on powder diffraction of the XV Congress of the IUCr, Toulouse, France, 1990.

Sasaki, K., Tanaike, O., and Konno, H.: Distinction of jarosite-group compounds by Raman spectroscopy, Can. Mineral., 36, 1225–1235, 1998.